Pergamon International Journal of Machine Tools & Manufacture 40 (2000) 1023–1038

INTERNATIONAL JOURNAL OF MACHINE TOOLS & MANUFACTURE DESIGN, RESEARCH AND APPLICATION

Nano-second laser pulse heating and assisting gas jet considerations

B.S. Yilbas *, S.Z. Shuja, M.O. Budair

Department of Mechanical Engineering, King Fahd University of Petroleum and Minerals, Dhahran 31261, Saudi Arabia

Received 19 May 1998; received in revised form 14 September 1999; accepted 12 November 1999

Abstract

The nano-second laser pulse gas assisting processing method offers considerable advantages in the heat treatment process. In the present study gas assisted nano-second pulse laser heating of a stationary surface is considered. The gas, which is air, impinging onto the workpiece surface is modelled using flow equations, while the low Reynolds number k–ϵ model is employed to account for the turbulence. A heat conduction equation is introduced for the solid heating. A numerical scheme using a control volume approach is employed when discretizing the governing equations. The simulation is repeated for two gas jet velocities. To validate the present predictions, an analytical solution accommodating the convection losses is introduced for the workpiece heating. It is found that the temperature profiles predicted from the simulations agree well with the analytical solutions. Moreover, impinging gas jet velocity has no significant effect on the temperature distribution in the workpiece. As the heating progresses, the equilibrium heating initiates, in which case the internal energy gain of the solid increases at an almost constant rate.

1. Introduction

Lasers can be used in many industrial processes including machining and surface treatment. Laser machining is characterized by a number of advantages, such as absence of tool wear, tool breakage, chatter, machine deflection, and mechanically induced machine damage [1–3]. The industrial usage of laser-based machining applications is dictated by the further development of improved and cost effective laser sources [4]. Laser machining is an extremely localized thermal process in which a certain portion of the incident beam energy is absorbed by the substrate and

* Corresponding author. Tel.: +966-3-860-2540; fax: +966-3-860-2949.
E-mail address: bsyilbas@kfupm.edu.sa (B.S. Yilbas).

PII: S0890-6955(99)00108-X

Nomenclature

a	coefficient of ϕ in Eq. (11)
b	Gaussian parameter
C_p	specific heat (J/kg K)
C_1, C_2, C_μ	coefficient, in the k–ϵ turbulence model
f_1, f_2, f_μ	coefficient in the low Reynolds number, k–ϵ model
G	rate of generation of k (W/m^3)
h	heat transfer coefficient (W/m^2 K)
I_0	peak power interlay (W/m^2)
K	variable thermal conductivity (W/m K)
k	turbulent kinetic energy (W/m^3)
p	pressure (Pa)
Re	Reynolds number
R	reflectivity
r	distance in the radial direction (m)
S	unsteady spatially varying laser heat source (W/m^3)
t	time (s)
T	temperature (K)
T_∞	free-stream temperature (K)
U	arbitrary velocity (m/s)
$\forall$	volume (m$_3$)
V	radial velocity (m/s)
W	axial velocity (m/s)
x	arbitrary direction (m)

Greek

α	thermal diffusivity (m^2/s)
δ	absorption coefficient (1/m)
ϵ	energy dissipation (W/kg)
λ	turbulence intensity
μ	variable dynamic viscosity (N s/m^2)
ν	variable kinematic viscosity (m^2/s)
ρ	density (kg/m^3)
σ	variable Prandtl number
τ	pulse length which is 1.08 ms
Φ	viscous dissipation (W/m^3)
ϕ	arbitrary variable

Subscript

i, j	arbitrary direction
jet	gas jet at inlet
l	laminar
o	constant properties
t	turbulent

heat is generated in the region of laser beam interaction. This results in material softening, local yielding, melting, burning or evaporation. Moreover, the heat transfer mechanism governing the laser treatment is extremely important, since the quality of the laser processing highly depends upon the thermal process. Modelling the physical process can yield much insight into the phenomena occurring within the region heated by the high-power laser beam. In addition, the modelling can substantially reduce the time required for process optimization, scale-up, and control.

A considerable number of analytical and numerical research works on the laser heating process have been carried out [5–7]. Simon et al. [8] studied heat conduction in deep penetration welding with a time modulated laser beam. They indicated that the time modulated laser beam had no significant influence on the resulting heat affected zone. Diniz Neto and Lima [9] computed non-linear temperature profiles due to pulsed laser heating. They discussed the applicability of the solutions to the actual laser pulse heating. Yilbas and Sami [10] investigated the laser repetitive pulse heating for a conduction limited process. He showed that pulse frequencies of the order of 1 kHz were needed for the thermal integration of the heating process. Moreover, Yilbas and Shuja [11] studied the pulsed laser heating process analytically and indicated that the equilibrium time was significantly affected by the pulse length employed.

Analytical and numerical modelling of solid substrate heating have contributed to the understanding of laser workpiece interaction, but there are other parameters including gas assisting jet affects that need to be considered. In laser thermal processing, a gas assisting, impinging co-axially with the laser beam, is used either to shield the workpiece from the oxygen environment or to generate an exothermic reaction enhancing the thermal process [12,13]. The effect of the gas assisting jet on the liquid layer thickness during laser cutting was investigated previously [14]. However, the effect of turbulence on the heating process was omitted and the information given on the viscous sublayer in the region close to the surface was not substantial. On the other hand, when a laser gas assisting process is modelled, the impinging turbulent jet should be accommodated. A considerable number of research studies were carried out on gas jet impingement, however, only a few considered the heat transfer from the impinging surface [15–17]. Craft et al. [17] carried out a simulation of four turbulence models in relation to gas jet impingement. They indicated that the Reynolds stress model predicted a flow field similar to that obtained from the experiment. A comprehensive review for circular jet impingement and heat transfer was carried out by Jambunathan et al. [18]. They indicated that the Nusselt number was independent of nozzle-to-plate spacing up to a value of 12 nozzle diameters at radii greater than six nozzle diameters from the stagnation point. Consequently, it becomes necessary to include the turbulent gas jet impingement when modelling the gas assisted heating process.

In the present study, numerical simulation of nano-second laser pulse heating of steel is carried out. Air is considered as an assisting gas, emerging from a nozzle and impinging co-axially with the laser beam onto the workpiece surface. Two-dimensional axisymmetric flow equations and an energy equation are solved numerically using a control volume approach, which in turn enables computation of the flow and temperature fields in the laser heated region. A low Reynolds number k–ϵ model is considered to account for the turbulence. To validate the theoretical predictions, an analytical solution is employed using the same conditions as the numerical simulation.

2. Modelling of gas jet impingement and laser heating

The fluid flow and heat transfer conditions are governed by the conservation principles of mass, momentum, and energy. However, the fluid flow is assumed as steady state before the laser heat source is switched on.

In the Cartesian tensor system, the continuity and momentum equations can be written in the following form:

$$\frac{\partial}{\partial x_i}(\rho U_i)=0 \tag{1}$$

and

$$\frac{\partial}{\partial t}(\rho U_j)+\frac{\partial}{\partial x_i}(\rho U_i U_j)=-\frac{\partial p}{\partial x_j}+\frac{\partial}{\partial x_i}\left[(\mu_t+\mu)\frac{\partial U_j}{\partial x_i}\right] \tag{2}$$

The eddy viscosity μ_t in the momentum equation has to be specified by a turbulence model. The partial differential equation governing the transport of thermal energy has the following form:

$$\frac{\partial T}{\partial t}+\frac{\partial}{\partial x_i}(\rho U_i T)=\frac{\partial}{\partial x_i}\left[\left(\frac{\mu_t}{\sigma_t}+\frac{\mu}{\sigma}\right)\frac{\partial T}{\partial x_i}\right]+\frac{\mu}{\rho C_p}\Phi \tag{3}$$

Equations governing the turbulent viscosity, μ_t, in Eqs. (2) and (3) can be defined using the two-equation k–ϵ model of turbulence. The turbulent viscosity is [19]:

$$\mu_t=C_\mu \rho k^2/\varepsilon \tag{4}$$

where C_μ, is an empirical constant and k is the *turbulence kinetic energy* which is given by

$$\frac{\partial}{\partial x_i}(\rho U_i k)=\frac{\partial}{\partial x_i}\left[\left(\frac{\mu_t}{\sigma_k}+\mu\right)\frac{\partial k}{\partial x_i}\right]+G-\rho\varepsilon \tag{5}$$

similarly ϵ is the *energy dissipation* which is given by the following differential equation

$$\frac{\partial}{\partial x_i}(\rho U_i \varepsilon)=\frac{\partial}{\partial x_i}\left[\left(\frac{\mu_t}{\sigma_\varepsilon}+\mu\right)\frac{\partial \varepsilon}{\partial x_i}\right]+\frac{\varepsilon}{k}(C_1 G-C_2\rho\varepsilon) \tag{6}$$

G represents the rate of generation of turbulent kinetic energy while $\rho\epsilon$ is its destruction rate. G is given by

$$G=\mu_t\left[\left(\frac{\partial U_i}{\partial x_j}+\frac{\partial U_j}{\partial x_i}\right)\frac{\partial U_i}{\partial x_j}\right] \tag{7}$$

The model contains six empirical constants which are assigned the following values:

$$C_\mu=0.09,\ C_1=1.44,\ C_2=1.92,\ \sigma_k=1.00,\ \sigma_\varepsilon=1.00$$

The k–ϵ model is only applicable when the flow is entirely turbulent. Close to the solid walls viscous effects become dominant, therefore, corrections in the k–ϵ model may be needed. This can be achieved by introducing a wall correction in the turbulence model.

2.1. Low Reynolds number k–ϵ correction

The Lam–Bremhorst low Reynolds number extension to the k–ϵ model employs a transport equation for the total dissipation rate. It differs from the standard high Reynolds number model in that the empirical coefficients C_μ, C_1, and C_2 are multiplied respectively by the functions:

$$f_\mu=(1-e^{-0.0165Re_l})^2\left(1+\frac{20.5}{Re_t}\right),\ f_1=1+\left(\frac{0.05}{f_\mu}\right)^3,\ f_2=1-e^{-Re_t^2}$$

where $Re_l=(y_n\sqrt{k})/\nu_l$, $Re_t=\kappa^2/\varepsilon\nu_l$ and y_n is the distance to the nearest wall. For high-turbulence Reynolds numbers, Re_l or Re_t, the functions f_μ, f_1, and f_2, multiplying the three constants, tend to unity.

2.2. Boundary conditions

The schematic view of the gas jet impingement is shown in Fig. 1. Four boundary conditions are required to solve the governing equations. The boundary conditions include inlet, outlet, solid surfaces and symmetry axis, which are given as follows.

2.2.1. Solid surface

The boundary conditions for U_i and T are

$$U_i=0,\ T=300\ \mathrm{K} \tag{8}$$

2.2.2. Low Reynolds number turbulence model

Laminar boundary conditions are set for the mean-flow variables, and the boundary conditions k=0 and $d\varepsilon/dy$=0 are applied at the wall. It should be noted that the low Reynolds number extension does not employ wall functions, and the flow field needs to be meshed into the laminar sublayer and down to the wall. The grid employed normal to the main flow direction needs to

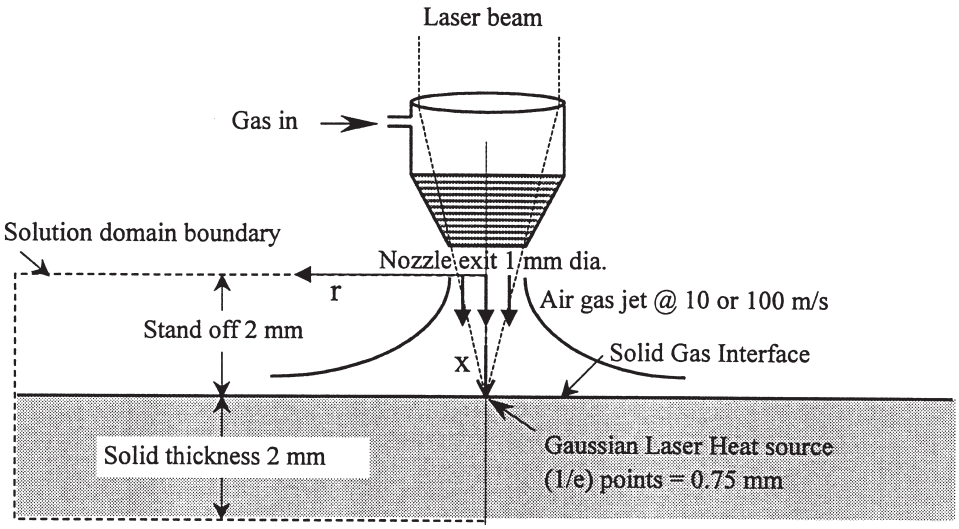

Fig. 1. Schematic view of jet impingement.

be distributed so as to give a high concentration of grid cells near the wall, with the wall-adjacent node positioned at y^+=1.0 or even less.

2.2.3. Inlet conditions

$$U_i=\text{specified}, \ T=300\ \text{K} \tag{9}$$

The kinetic energy of turbulence is estimated according to a certain percentage of the square of the average inlet velocity:

$$k=\lambda\bar{u}^2 \tag{10}$$

where $\bar{u}$ is the average inlet velocity and λ is a percentage.

The dissipation is calculated according to the equation

$$\varepsilon=C_\mu\frac{k^{\frac{3}{2}}}{aD} \tag{11}$$

where D is the inlet diameter. The values λ=0.03 and a=0.005 are commonly used and may vary slightly in the literature [20].

2.2.4. Outlet conditions

It is assumed that the flow extends over a sufficiently long domain so that it is fully developed at the exit section. Thus, for any variable ϕ the condition is

$$\frac{\partial\phi}{\partial x}=0 \tag{12}$$

where x is the arbitrary outlet direction.

2.2.5. Symmetry axis

The radial derivative of the variables is set to zero, i.e.

$$\frac{\partial\phi}{\partial r}=0 \tag{13}$$

2.2.6. Solid fluid interface

Continuity of the temperature is assumed, apart from the condition for the solid wall.

2.3. Governing equations for the laser heated solid plate

The transient heat conduction in a stationary medium is considered for the laser heated solid surface. Therefore, the unsteady heat conduction equation becomes a simplification of Eq. (3) with the addition of an unsteady term and a laser heat source term, i.e.

$$\frac{\partial}{\partial t}(c_{\mathrm{p}}\rho T)=\frac{\partial}{\partial x_i}\left[K\frac{\partial T}{\partial x_i}\right]+S \tag{14}$$

where S is the unsteady spatially varying laser output power intensity distribution and is considered as Gaussian with $\frac{1}{\mathrm{e}}$ points equal to 0.375 mm, i.e. the radius of the laser heated spot, from the center of the beam. Therefore:

$$S=\frac{1}{\sqrt{2\pi a}}I_o\delta\exp\left(-\frac{r^2}{a^2}\right)\exp(-\delta\cdot z)H(t-\tau)$$

where I_o is the peak power intensity and a is the constant. H is the heaviside function which is used to define the pulse length. The step input laser pulse is considered for simplicity, with the pulse length τ=2 ns.

2.3.1. Boundary conditions in connection with the solid plate heating

Convection with a constant coefficient for still air is considered at the $z=z_{\max}$ boundary for the solid plate. At the interface, continuity of temperature between the solid and the gas is enforced; far away from the laser source, constant temperature T=300 K is assumed.

3. The numerical technique

The algebraic equations are derived for the grid-point values of the variables from the differential equations governing the relevant variables. The calculation domain is divided into subdomains or control volumes such that there is one control volume around a grid point. The differential equation is integrated over the control volume to yield the discretization equation. The control volume approach can be regarded as a special case of the method of weighted residuals in which the weighting function is chosen to be unity over a control volume and zero everywhere else. The main reasons for choosing the control volume formulation are its simplicity and easy physical interpretation. The details of the control volume approach are not given here due to the lengthy arguments involved, but it can be found in [21]. A semi-implicit method for pressure linked equations (SIMPLE) algorithm is used when handling the pressure linkages through the continuity equation [21].

3.1. Grid generation and computation

The computations were performed for a rectangular box-shaped domain around the jet. The calculation domain was chosen such that, in the r direction, it extended from the symmetry plane to a location where r/r_j, had a value of 10, therefore, the jet velocity there became almost parallel to the radial direction. In the flow field along the z direction, one boundary of the domain coincided with the laser heated solid placed two jet diameters from the jet center and the other boundary with the jet outlet.

The computer program used in this work had the capability of handling a nonuniform grid spacing. In each direction, fine grid spacing near the injection point and the laser heated spot was allocated while gradually increasing spacing was allocated for locations away from the origin. The grid generated in the present study is shown in Fig. 2. The number of grid planes used normal to the y and z directions were 38 and 70, respectively, thus making a total of 2660 grid points. Trials on a 43×100 grid produced results which were within 2% of those from the 38×70 grid, as shown in Fig. 2.

As for the dependent variables, seven quantities were computed at all grid points; these were: the three velocity components, the local pressure, the two turbulence quantities, and the temperature. The iterations were terminated when, from one iteration to the next, the change in the value of each local velocity was less than 0.2% of the main stream velocity. In this manner, about 300 iterations were needed for each run.

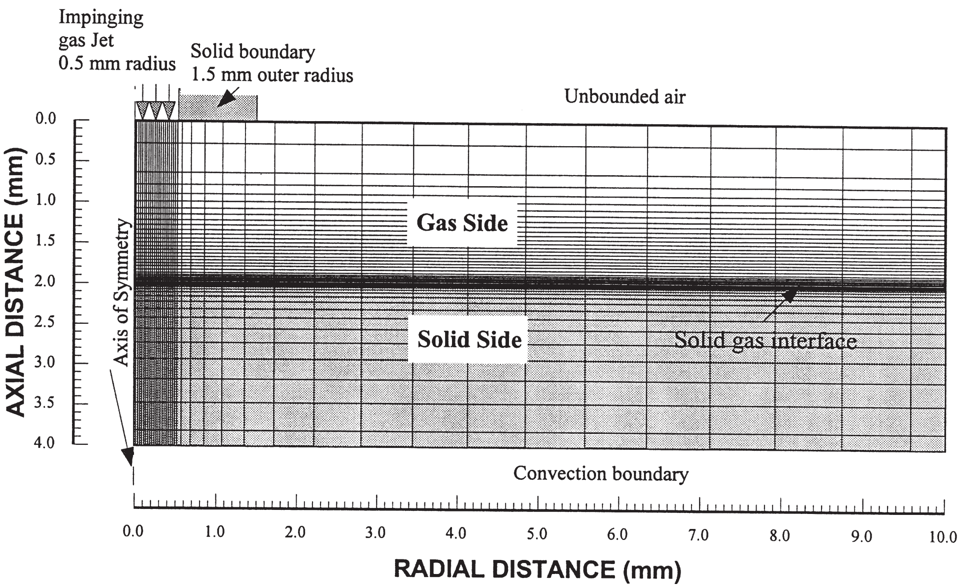

Fig. 2. Grid generated for numerical simulation.

4. Analytical solution to laser heating including the convective losses

In order to validate the present predictions, a one-dimensional analytical solution of the heat transfer equation is considered. In this case, the present predictions are simulated for constant properties. This is because that the closed form analytical solution was obtained for constant properties [22]. The one-dimensional heat conduction equation for a solid with constant properties can be written as:

$$\rho_o Cp_o \frac{\partial T}{\partial t} = K_o \frac{\partial^2 T}{\partial x^2} + I_o(1-R)\exp(-\delta x) \tag{15}$$

where R, I_o, K_o, ρ_o, and Cp_o are the surface reflectivity, peak power intensity, constant thermal conductivity, constant density, and constant specific heat capacity at constant pressure.

The appropriate boundary conditions are:

$$\frac{\partial T}{\partial x} = \frac{h}{K_o}(T_s - T_\infty) \tag{16}$$

and

$$\frac{\partial T(\infty, t)}{\partial x} = 0$$

where h and T_s are the heat transfer coefficient and the surface temperature.

The initial condition is:

$$T(x, 0) = 0$$

The solution of this equation is reported in the literature [22]. The temperature distribution in the substrate having an initial temperature of zero is:

$$T(x,t) = \frac{I_o(1-R)}{\delta K_o}\left[\left(1+\frac{\delta K_o}{h}\right)\operatorname{erf} c\left(\frac{x}{2\sqrt{\alpha_o t}}\right) + \frac{1}{\frac{h}{\delta k_o}\left(\frac{h}{\delta k_o}-1\right)}\exp\left(\frac{h^2}{K_o^2}\alpha_o t + \frac{hx}{K_o}\right)\operatorname{erf} c\left(\frac{x}{2\sqrt{\alpha_o t}}\right) + \frac{h}{k}\sqrt{\alpha_o t}\right] \tag{17}$$

The computer program is developed to determine the temperature profiles from the equation for stainless steel. The thermal properties of air and stainless steel used in the computation are given in Table 1.

Table 1
Property table

Property		Gas (air)	Solid (steel)
Density	ρ (kg/m^3)	p/RT	7836
Thermal conductivity	K (W/mk)	$0.008103274+6.04893\times10^{-5}T$	$64.102-0.04803T+1.518\times10^{-5}T^2$
Specific heat capacity	c_p (J/kg K)	$917+0.258T+3.9804\times10^{-5}T^2$	$24.558+1.223T-0.37693\times10^{-3}T^2$
Kinematic viscosity	ν (m^2/s)	$-0.494679\times10^{-5}+0.458394\times10^{-7}T$ $+0.80974\times10^{-10}T^2$	-

5. Results and discussions

In the present study, the simulations are carried out for a nano-second laser pulse heating and two assisting gas jet velocities. The predictions are introduced for temperature and flow fields under the relevant sub-headings.

5.1. Temperature field predictions

Fig. 3 shows the temperature contours in the gas and solid substrate, which are obtained at different heating times for 10 and 100 m/s gas jet velocities. Temperature in the solid side gradually decays as the distance from the surface increases. Moreover, temperature builds up close to the surface vicinity as the heating progresses. The effect of gas jet velocity on the solid side temperature is negligible. This may suggest that the internal energy gain during the heating cycle dominates the convection losses from the solid surface. In the gas side, temperature profiles extend further into the gas in the surface vicinity. As the heating progresses the gas side temperature close to the laser heated region increases considerably, which in turn results in heating of the impinging gas in this region, i.e. due to the convection mixing the size of the heated spot is extended in the surface vicinity.

Fig. 4 shows the temperature profiles in the axial direction inside the substrate obtained from numerical predictions and analytical solution. The temperature decay rate in the substrate during the early heating period is higher than the corresponding rate as the heating progresses. This may be because of the internal energy gain of the substrate, which is higher than the conduction losses in the early heating period. The influence of assisting gas jet velocity has no significant effect on the resulting temperature profiles. When comparing the numerical results with analytical findings, it is apparent that both results are in good agreement. However, the small discrepancies in both results at some depth inside the substrate is because of the initial conditions introduced before the laser heating process, i.e. stagnation heating due to impinging gas raises the substrate temperature slightly before the initiation of laser heating.

Fig. 5 shows the temporal variation of the surface temperature due to two gas jet velocities. The cooling effect of the assisting gas jet on the resulting surface temperature is negligible. This may be because of the small size of the irradiated area and the low heat transfer coefficient, which is of the order of 10^7 W/m^2 K, developed at the surface for these particular gas assisting jet velocities. Consequently, both curves coincide. The surface temperature rises at a faster rate in the pulse beginning than in the late phase of the heating. This is also evident from Fig. 6, in

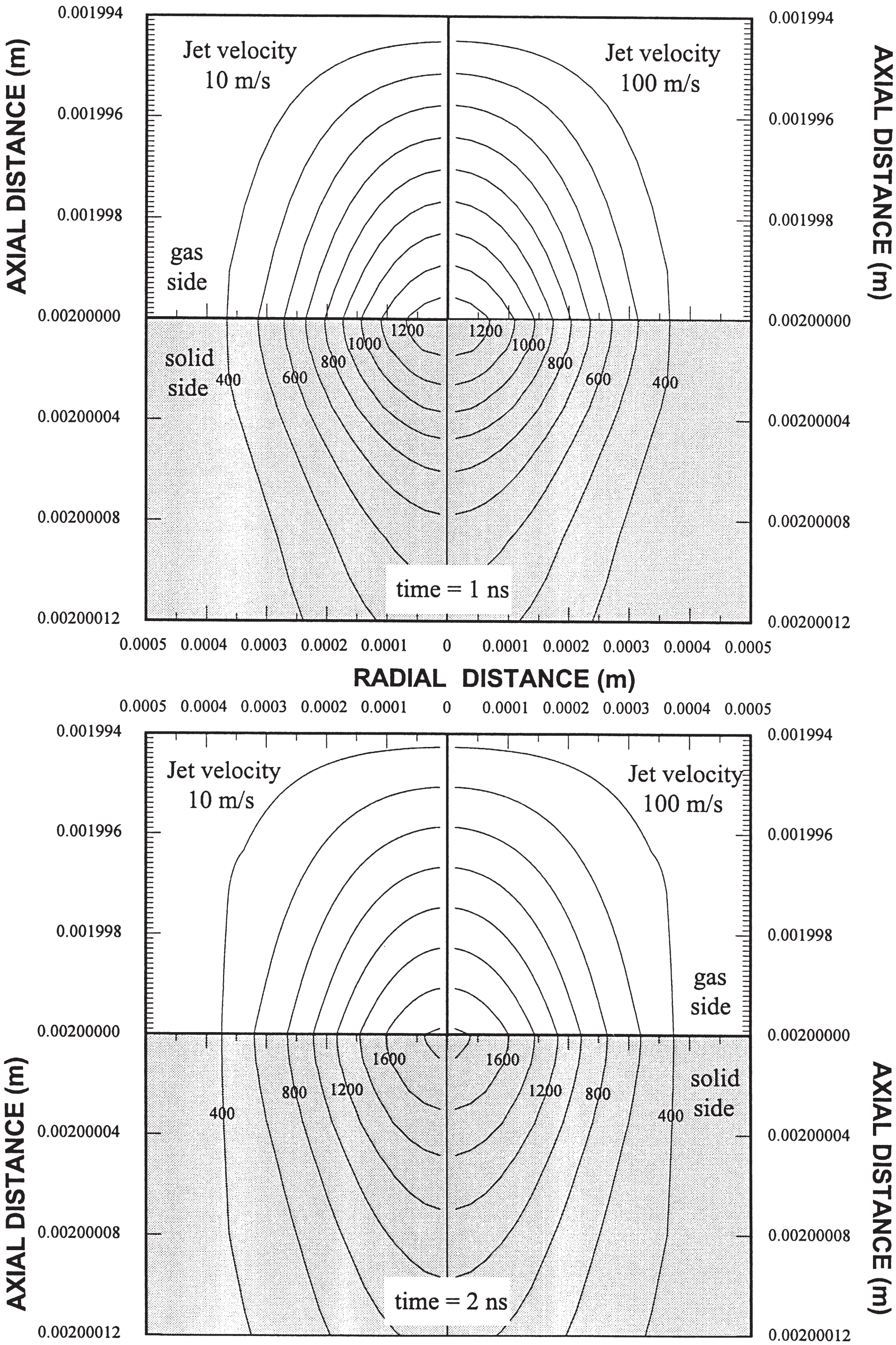

Fig. 3. Temperature contours in the solid and gas sides for 10 and 100 m/s gas jet velocities and at different heating times, I_o=3.0×10^{19}.

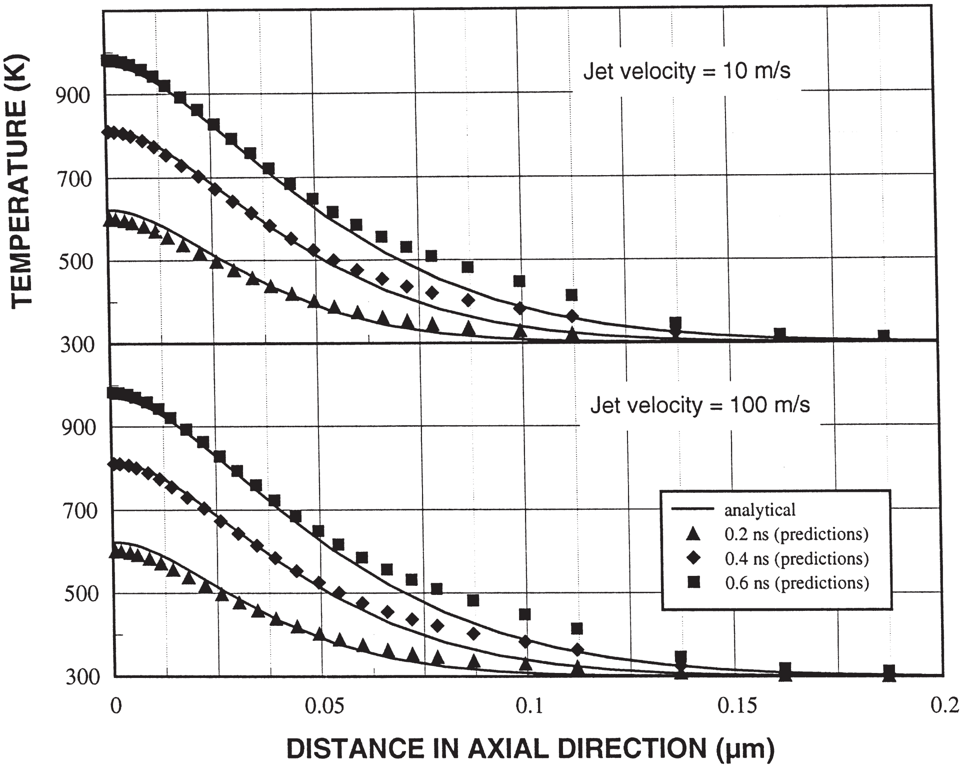

Fig. 4. Temperature distribution in the solid obtained from the present simulation and the analytical solution by Blackwell [22] with nano-second pulse and for two gas jet velocities.

which $\partial T/\partial t$ variation with time is shown. In this case, the internal energy gain dominates the conduction losses, resulting in a rapid rise in the surface temperature. As the heating progresses, the rise in surface temperature remains almost constant. This may indicate that the energy absorbed due to the laser beam balances the internal energy gain, conduction, and convection losses such that the rate of the internal energy gain remains constant, i.e. equilibrium heating is the dominating mechanism. In the cooling cycle, the surface temperature decays at a faster rate immediately after the pulse end compared to some time after the pulse ending.

5.2. Flow field predictions

Figs. 7 and 8 show the pressure and radial (V) and axial (W) velocity contours for two gas assisting jet velocities, respectively. The pressure attains high values in the surface vicinity for 100 m/s gas jet velocity. As the distance in the axial direction (z direction) increases, both pressures corresponding to the two gas assisting jet velocities become similar. When examining Fig. 8, it may be observed that the U velocity attains higher values in the surface vicinity for 100 m/s gas jet velocity than the values corresponding to 10 m/s velocity. In this case, the radial pressure gradient developed in the stagnation region is considerably higher at 100 m/s gas jet velocity, which in turn increases the radial flow in this region. However, the radial flow developed does

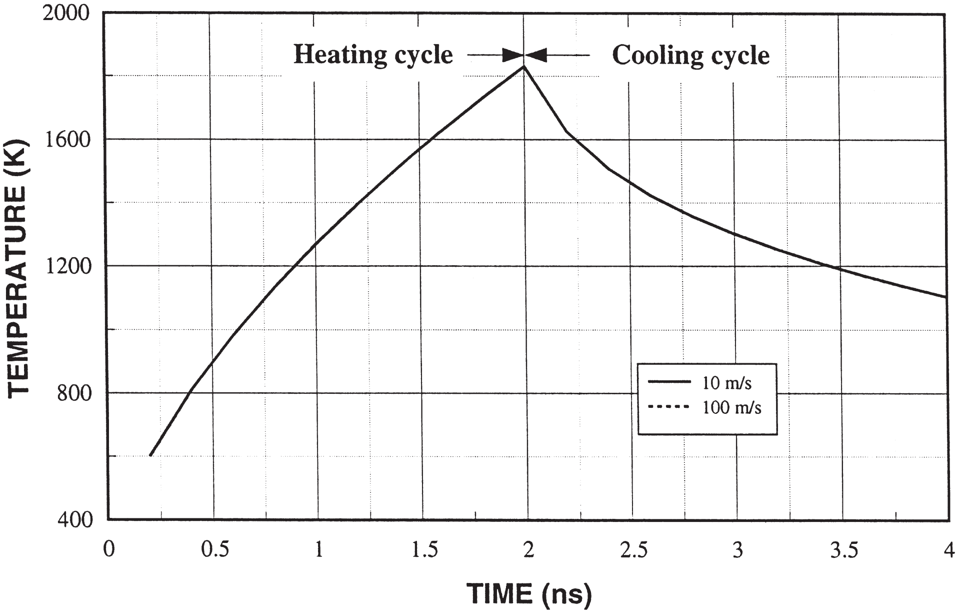

Fig. 5. Variation of surface temperature with time at the center of the heated spot (both curves coincide).

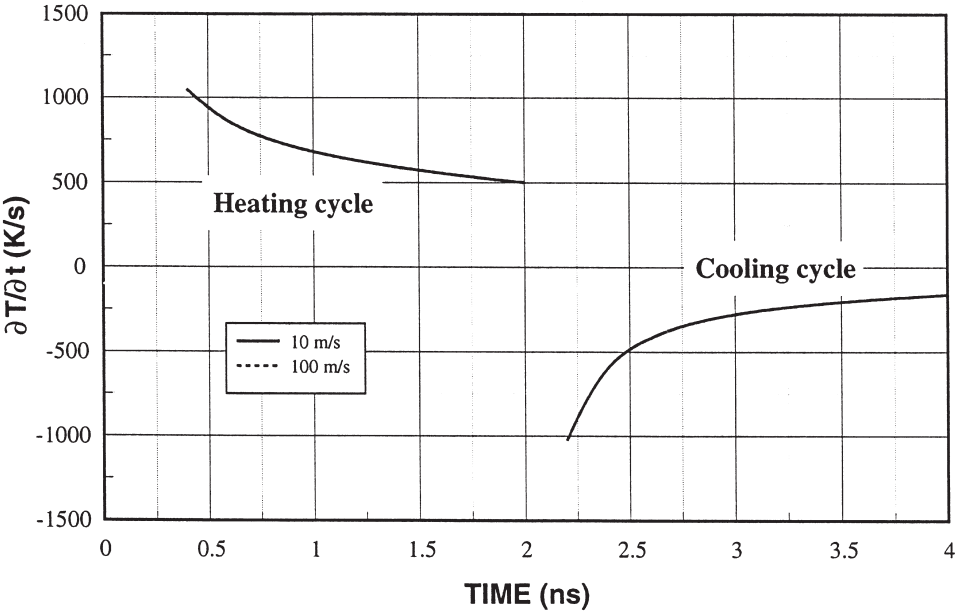

Fig. 6. Variation of $\partial T/\partial t$ with time at the center of the heated spot (both curves coincide).

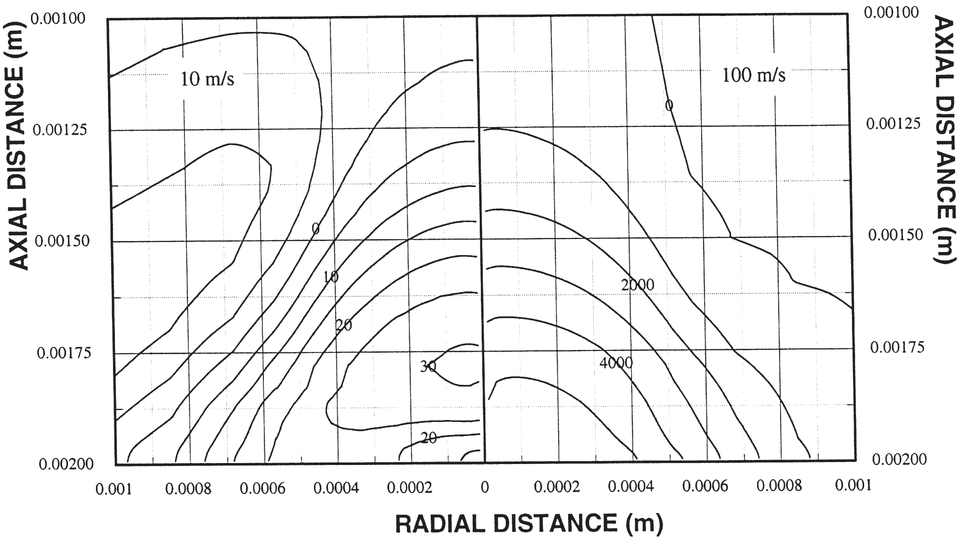

Fig. 7. Pressure contours obtained for two gas jet velocities, time=0.2 ns. The unit of pressure is Pascal (gauge).

not result in a sufficiently high heat transfer coefficient across the heated surface. Consequently, the surface temperature remains almost constant at all impinging gas jet velocities. In addition, considerable variation is observed in the axial velocity contours at different gas assisting jet velocities. This may be because of the different flow fields developed for different impinging gas jet velocities.

6. Conclusions

The conclusions derived from the present work may be listed as follows:

1. The impinging gas jet velocity considered at present has no influence on the solid side temperature profiles for nano-second laser pulse heating. However, the gas side temperature in the surface vicinity varies considerably when the assisting gas jet velocity is changed. In this case, the heat transfer coefficient developed at the surface is not high enough to alter the solid surface temperature.
2. The surface temperature rises at a fast rate in the laser pulse beginning, in which case the internal energy gain dominates the conduction and convection losses. As the heating progresses, internal energy increases at a constant rate, which in turn results in the attainment of equilibrium heating.
3. The temperature profiles inside the substrate, which were predicted numerically and analytically, are in good agreement. Moreover, some small discrepancies in both the profiles at some depth below the surface are due to the consideration of stagnation point heating before the initiation of laser heating in the numerical simulation, i.e. the solid substrate is heated before the laser is switched on.
4. A high pressure region is developed in the surface vicinity at 100 m/s gas jet velocity, which

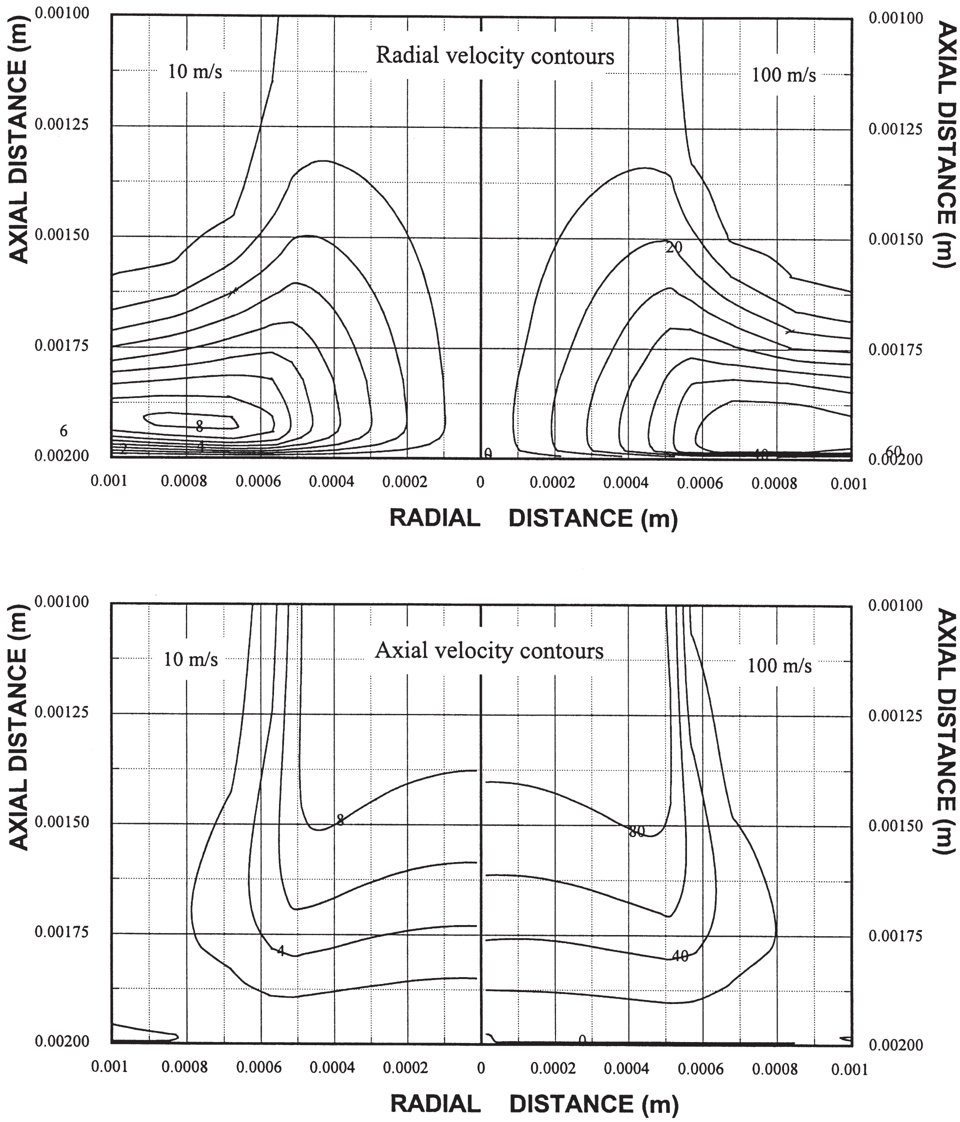

Fig. 8. Velocity contours obtained for two gas jet velocities; time=0.2 ns.

in turn results in increased radial flow in the surface vicinity. This influences considerably the gas side temperature distribution in this region. However, the radial flow developed is not substantial enough to result in a high heat transfer coefficient at the workpiece surface that would influence the surface temperature.

Acknowledgement

The authors acknowledge the support of King Fahd University of Petroleum and Minerals Dhahran, Saudi Arabia for this work.

References

[1] B.S. Yilbas, Study of affecting parameters in laser hole drilling of sheet metals, Transactions ASME: Journal of Engineering Materials Technology 109 (1987) 282–287.
[2] R.C. Crafer, P.J. Oakley, Laser Processing in Manufacturing, Chapman and Hall, London, 1993.
[3] W.W. Duley, CO_2 Laser Effects and Applications, Academic Press, New York, 1976.
[4] D. Leidinger, A. Penz, D. Schnocker, Improved manufacturing processes with high power lasers, Infrared Physics Technology 36 (1) (1995) 251–256.
[5] P.A. Molian, Dual beam CO_2 laser cutting of thick metallic material, Journal of Material Science 28 (1993) 1738–1748.
[6] B.S. Yilbas, A. Sahin, Laser heating mechanism including evaporation process initiating laser drilling, International Journal of Machine Tools and Manufacturing 35 (1995) 1047–1062.
[7] B.S. Yilbas, Laser heating process and experimental validation, International Journal of Heat and Mass Transfer 40 (5) (1997) 1131–1143.
[8] G. Simon, U. Gratzke, J. Kroos, Analysis of heat conduction in deep penetration welding with a time-modulated laser pulse, Journal of Physics D: Applied Physics 26 (1993) 862–869.
[9] O. Diniz Neto, C.A.S. Lima, Nonlinear three-dimensional temperature profiles in pulsed laser heated solids, Journal of Physics D: Applied Physics 27 (1994) 1795–1804.
[10] B.S. Yilbas, M. Sami, Thermal integration in laser pulse heating — a kinetic theory approach, Journal of Physics D: Applied Physics 30 (22) (1997) 3088–3095.
[11] B.S. Yilbas, S.Z. Shuja, Heat transfer analysis of laser heated surfaces — conduction limited case, Applied Surface Science 108 (1997) 167–175.
[12] J.T. Powell, T.G. King, I.A. Mencies, Cut, edge quality improvements by laser pulsing, in: Proceeding of 2nd International Conference on Lasers in Manufacturing, Birmingham, UK, 1985, pp. 37–45.
[13] B.S. Yilbas, A.Z. Sahin, Turbulent boundary layer approach allowing chemical reactions for CO_2 laser oxygen-assisted cutting process, Proceedings Institution of Mechanical Engineers 208 (1994) 275–284.
[14] J.W. Baugh, S. Shimizu, Heat transfer measurements from a surface with uniform heat flux and an impinging jet, ASME Journal of Heat Transfer 111 (1989) 1096–1098.
[15] R. Gordon, J.C. Akfirat, The role of turbulence in determining the heat transfer characteristics of impinging jets, International Journal of Heat and Mass Transfer 8 (1965) 1261–1272.
[16] B.R. Hollworth, L.R. Geo, Entrainment effects on impingement heat transfer: part 2 — local heat transfer, ASME Journal of Heat Transfer 107 (1985) 910–915.
[17] T.J. Craft, L.J.W. Graham, B.E. Launder, Impinging jet studies for turbulence model assessment — II. An examination of the performance of four turbulence models, International Journal of Heat and Mass Transfer 36 (10) (1993) 2685–2697.
[18] K. Jambunathan, E. Lai, M.A. Moss, B.L. Button, A review of heat transfer data for single circular jet impingement, International Journal of Heat and Fluid Flow 13 (1992) 106–115.
[19] H.K. Versteeg, W. Malalasekera, An Introduction to Computational Fluid Dynamics, The Finite Volume Method, Longman Scientific and Techinical, 1995.
[20] D. Elkaim, M. Reggio, R. Camarero, Simulating two-dimensional turbulent flow by using the k–ϵ model and the vorticity-stream function formulation, International Journal for Numerical Methods in Fluids 14 (1992) 961–980.
[21] S.V. Patankar, Numerical Heat Transfer, McGraw-Hill, New York, 1980.
[22] B.F. Blackwell, Temperature profile in semi-infinite body with exponential source and convective boundary conditions, Journal of Heat Transfer 112 (1990) 567–571.